Investigation of anisotropy as a possible cause for an AVO pitfall: *post-mortem* analysis

Cristiano Icaro Rego Nunes, Lucas Mesz, Alberto Lopes de Carvalho, Vinicius Ferreira Carneiro – Petróleo Brasileiro S/A

This paper was prepared for presentation during the 16th International Congress of the Brazilian Geophysical Society held in Rio de Janeiro, Brazil, 19-22 August 2019.

Abstract

During *post-mortem* analysis of a prospect drilled offshore Brazil that found no hydrocarbons, despite showing very promising AVO anomalies, we decided to investigate if anisotropy could be one of the reasons for this pitfall. This work summarizes our efforts in reprocessing, modelling and interpretation in order to study the influence of anisotropy over the seismic data. We show that the relatively high values of Thomsen's parameters Delta and Epsilon estimated for the shale layer above the reservoir can completely change the AVO response in this area and produce anomalies even for a water-saturated rock, showing that anisotropy must not be disregarded during AVO analysis.

Introduction

The well was seeking for oil-saturated sandstones based on RMS amplitude maps and AVO (Amplitude Variation with Offset) type III anomalies. Figure 1 shows Near, Mid and Far offset sections near the well. These data came from an isotropic, Post-Stack Time Migration (PSTM) volume.

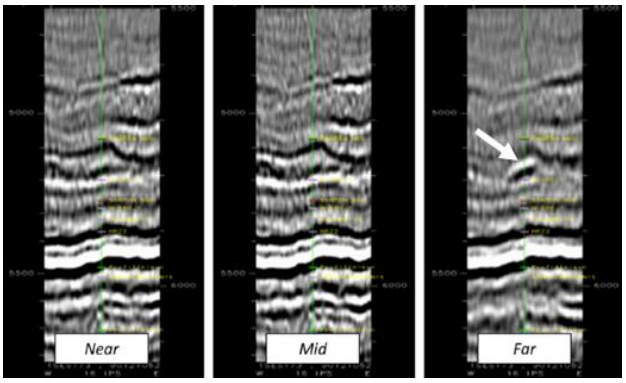

Figure 1: PSTM (Near, Mid and Far) sections near the well (green line). The anomaly is clear in the Far section, as indicated by the white arrow.

The well discovered a water-saturated sandstone whose 1D isotropic synthetic response (Figure 2) did not agree with the response from the seismic, especially at far offsets. This was a hint that something else was affecting the amplitudes. Among other possibilities, anisotropy has come up as a possible explanation for this divergence.

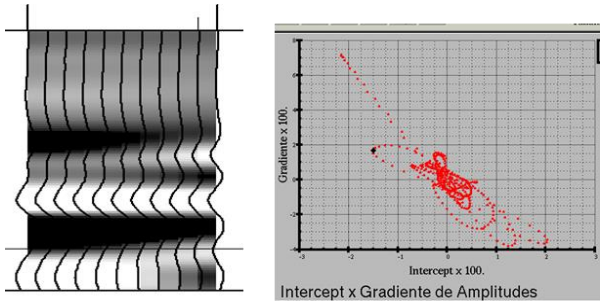

Figure 2: synthetic isotropic seismogram (0-42°) at the reservoir level and intercept-gradient crossplot showing AVO type IV response (black dot), different from the AVO type III seen in the PSTM image (Figure 1).

Theory and Method

Seismic anisotropic media have wave propagation velocities varying with propagation direction. Thus, a wavefront generated by a point source may be non-spherical (even in homogeneous media) and a ray may be non-perpendicular to the wavefront, travelling then through a different path than it would in isotropic media. Anisotropy may be intrinsic (inherent to the minerals and/or crystals of the rock) or extrinsic (due to multiple thin isotropic layers whose single effect can not be distinguished in seismic scale). In fact, Backus (1962) showed that an extrinsically anisotropic medium, for long waves, behaves like a transversely isotropic (TI) homogeneous medium.

Later, Thomsen (1986) described a vertical transversely isotropic (VTI) medium in terms of P-wave and S-wave velocities (V_P and V_s) along the vertical axis of symmetry and three non-dimensional parameters δ (Delta), ε (Epsilon) and γ (Gamma) defined in terms of the elastic coefficients c_{ij} that relate stresses and strains according to Hooke's law. Under the condition of weak anisotropy ($\delta, \varepsilon \ll < 1$):

$$V_h \approx V_{p0}\,(1+\varepsilon)$$
$$V_{NMO} \approx V_{p0}\,(1+\delta)$$

In the equations above, V_h is the horizontal P-wave velocity, V_{p0} is the vertical P-wave velocity and V_{NMO} is the Normal-Moveout (NMO) velocity. Epsilon indicates the contrast between horizontal (usually faster) and vertical P-wave velocities, while Delta indicates the contrast between NMO and vertical P-wave velocities. Gamma is related to the contrast between fast and slow S-wave velocities, but it is not considered in this work.

These parameters modify the expression of reflection coefficient as a function of incidence angle (θ) and affect the traditional AVO analysis. Exact equations for reflection and transmission coefficients in VTI media (R_{PP}^{VTI}) may be found in Daley & Hron (1977). An approximate expression, adding anisotropy effects to the traditional AVO coefficients, was given by Ruger (1997):

$$R_{PP}^{VTI}(\theta) = A_{iso} + (B_{iso} + \Delta\delta)\, sen^2(\theta) + (C_{iso} + \Delta\varepsilon)\, sen^2(\theta) tan^2(\theta)$$

A_{iso}, B_{iso} and C_{iso} represent the traditional terms of intercept, gradient and curvature of classic isotropic AVO analysis (e.g. Shuey, 1985) and depend on densities and P and S-wave velocities above and below the interface under analysis.

From Ruger's equation, it is clear that the variation of Delta affects the gradient term, which controls mainly the near and mid offsets amplitudes, while the variation of Epsilon changes the curvature term, which affects mainly the long offsets. The intercept term does not change in VTI media. Approximate expressions for the reflection coefficient in TTI (Tilted Transversely Isotropic) media can be found in Ivanov & Stovas (2015) (spoiler: the intercept term also changes).

Therefore, anisotropy is capable of changing in a non-negligible way the AVO response and potentially produce pitfalls. This potential effect is the object of investigation of this work.

For this investigation, we decided to reprocess a small volume around the well, assuming VTI symmetry. In order to aid interpretation, we used the outputs (Velocity, Delta, Epsilon) of re-processing as inputs for a ray-tracing software to generate synthetic seismograms under different scenarios (water and oil-saturated sandstones) and study how amplitudes would behave.

Results

Alkhalifah & Tsvankin (1995) defined a new anisotropic parameter called Eta (η) as follows:

$$\eta = \frac{1}{2}\left(\frac{{V_h}^2}{{V_{NMO}}^2} - 1\right) = \frac{\varepsilon - \delta}{1 + 2\delta}$$

For TI media, only Eta and the short-spread NMO velocity (V_{NMO}) are sufficient for all time processing (Alkhalifah & Tsvankin, 1995) using the 4th order approximation of traveltime equation (where X represents the offset, t the traveltime and t_0 the zero-offset traveltime):

$$t^2 = {t_0}^2 + \frac{X^2}{{V_{NMO}}^2} - \frac{2\eta\, X^4}{{V_{NMO}}^2({t_0}^2 {V_{NMO}}^2 + [1 + 2\eta]X^2}$$

We first performed PSTM processing, with joint V_{NMO} and effective Eta (η_{eff}) picking. We then converted the Eta field to an interval Eta field using the following relation (Alkhalifah, 1997), where $\varphi = 1 + 8\,\eta_{eff}$:

$$\eta_{(i)} = \frac{1}{8}\left[\frac{\varphi V_{NMO(i)}^4 t_{0(i)} - \varphi V_{NMO(i-1)}^4 t_{0(i-1)}}{V_{NMO(i)}^4 (t_{0(i)} - t_{0(i-1)})} - 1\right]$$

For Epsilon and Delta, we assumed $\varepsilon = 2\delta$ as an initial guess based on previous experience. Figure 3 and Figure 4 show, respectively, an inline section of interval Eta and Delta:

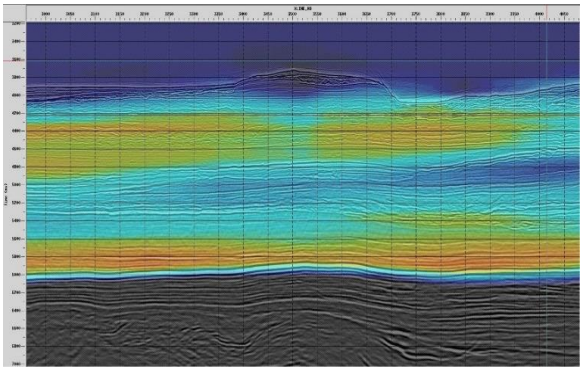

Figure 3: interval Eta field. Highest values reach 11,5%.

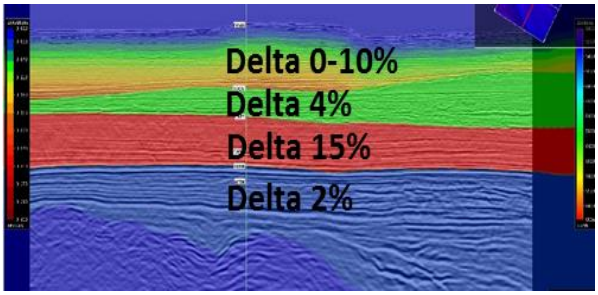

Figure 4: Delta field. Four "layers" could be distinguished. High values (reaching 15%) were estimated for the shale layer above the reservoir.

We also ran three iterations of isotropic tomography in order to estimate, via well markers, Delta values and compare them with the previous ones. For this, we used the following relation, where ΔZ_s is the thickness of a layer in the isotropic-migrated seismic and ΔZ_w is the thickness of the same layer in the well (Tsvankin, 2001):

$$\delta = \frac{1}{2}\left[\left(\frac{\Delta Z_s}{\Delta Z_w}\right)^2 - 1\right]$$

With this method, we obtained ~5% for the shallow layer, ~4% for the second layer and ~12% for the third layer (the most anisotropic), reasonably compatible with the values shown in Figure 4.

We then ran five iterations of VTI tomography and performed a Kirchhoff PreStack Depth Migration (PSDM), whose final image is shown in Figure 5. Figure 6 shows three Common Image Gathers (CIG) near the well position and the synthetic isotropic seismogram (0-42°), again showing poor correlation in long offsets. Figure 7 presents the intercept-gradient crossplot, highlighting, as the previous processing, an AVO type III anomaly with high deviation from the background trend.

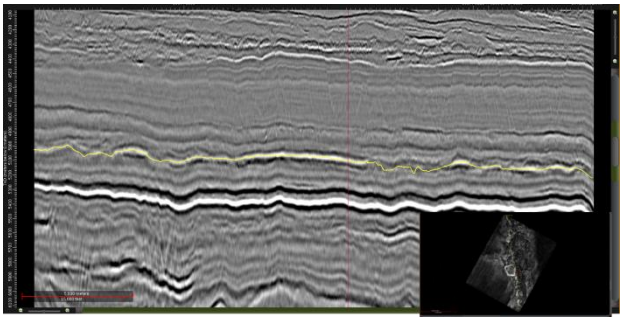

Figure 5: final PSDM image. The yellow event is the top of reservoir and the red line shows the well position.

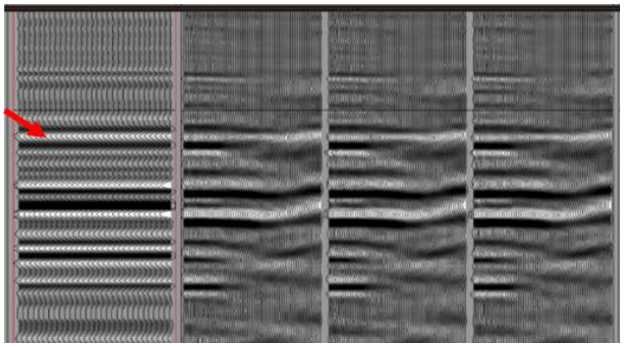

Figure 6: synthetic isotropic seismogram (left) and three common image gathers near the well position. The arrow indicates the top of reservoir. The real AVO response is not modelled by the isotropic seismogram.

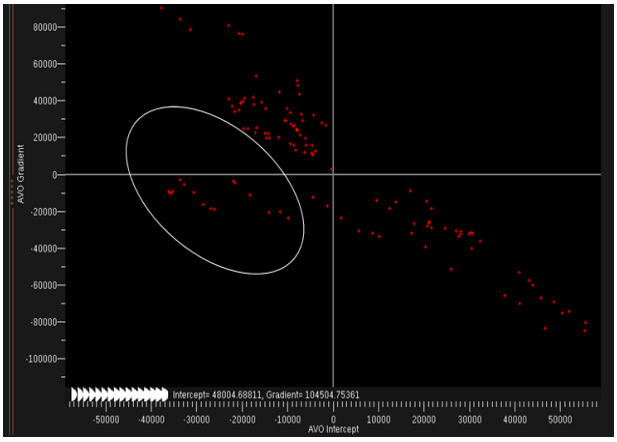

Figure 7: intercept - gradient crossplot. The top of reservoir appears as a high-deviation AVO type III anomaly.

We then used ray-tracing modelling to help understand the amplitude behaviors. The accuracy losses related to the smoothing requirements of the method are largely compensated by the computation time and flexibility (we could, for example, generate synthetic seismograms considering only the reflection at the top of reservoir).

We built two smooth macro-models (one isotropic, one VTI) with the properties volumes generated by the reprocessing. At the reservoir level, the VTI model has anisotropic shale over isotropic sandstone, producing Delta and Epslion contrasts that, according to Ruger's equation, will change the AVO response, as we will show soon.

Figures 8 and 9 show a fan of rays reaching the same point at the top of reservoir for the isotropic and the VTI model, respectively. It can be seen that rays travel through different paths in subsurface, which will affect kinematic attributes such as traveltimes and incidence angles.

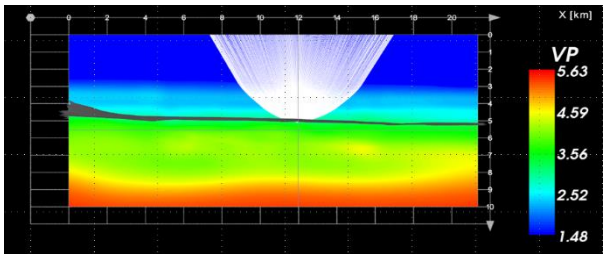

Figure 8: a fan of rays reaching a point at the top of reservoir, traced over an isotropic model.

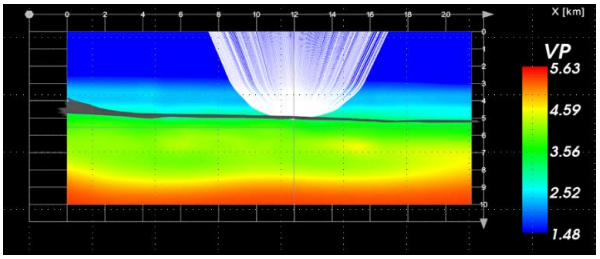

Figure 9: the same fan of rays traced over the VTI model. Anisotropy changes the raypaths.

We then generated synthetic CMP (Common MidPoint) gathers for the isotropic and VTI models from a source line passing through the well position. As shown in Figure 10, the VTI model presents amplitude variation with offset much closer to the real data (Figure 6).

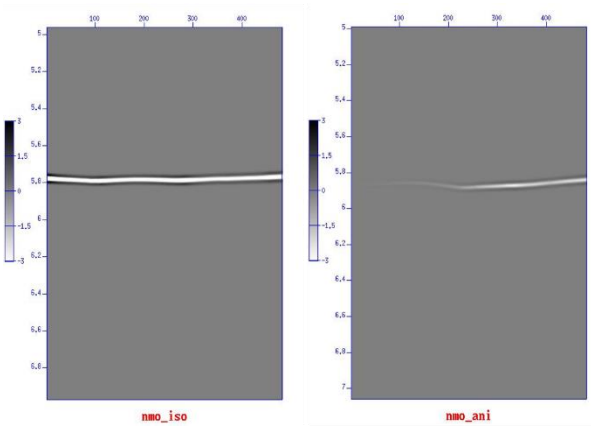

Figure 10: CMP gathers generated from a source line next to the well position for the isotropic model (left) and the VTI model (right). Amplitude behavior is reasonably similar to those in Figure 11a. The VTI gather is much closer to the real reprocessed data (Figure 6).

We also used a reflectivity calculator to check if amplitude behavior was consistent with Zoeppritz equations. In Figure 11a, we show the expected reflection coefficient varying with incidence angle for the values found in the

smooth model, above and below the target. In Figure 11b, we picked amplitudes of a shot gather near the well position and plotted them against offset. The comparison between the two curves should be made with care: although correlated, reflection coefficient is not amplitude and incidence angle is not offset. One of the possible effects of this mismatch is stretching of the horizontal scale. However, in relatively simple geologic models, it is expected that both curves behave similarly and this is what happens in Figure 11.

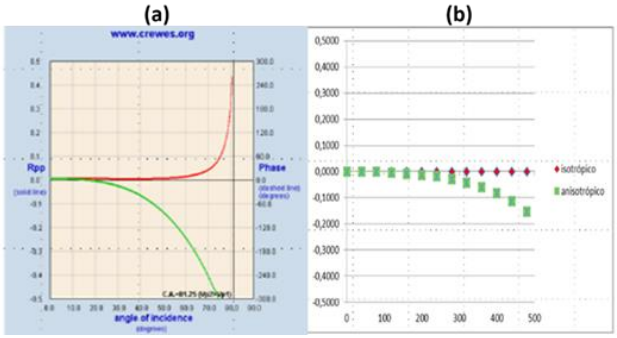

Figure 11: (a) isotropic (red) and VTI (green) reflection coefficients curves calculated from values found in the smooth model. (b) Amplitudes picked in a shot gather close to the well position. Modelled amplitudes show coherent behavior with Zoeppritz equations and the VTI model shows an amplitude anomaly in the far offsets.

Figures 10 and 11 alone are sufficient to show how anisotropy can completely change AVO behavior, since isotropic and VTI synthetic gathers are very different, with the latter much more loyal to real data. However, one could argue that the smooth model we used may not properly represent the sharp impedance contrasts at the reservoir level.

To overcome this, we took advantage of ray-tracing flexibility to insert, below the top of reservoir, properties values found in the well, representing a water-saturated scenario. We then calculated the reflectivity curves and picked amplitudes in the same shot gather of Figure 11. The result is shown in Figure 12. Then we used Gassmann's equations to do a fluid substitution simulation and generate an oil-saturated scenario, for which we did the same procedure. The result is shown in Figure 13.

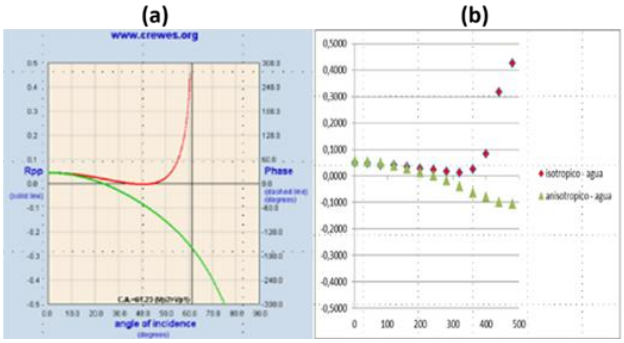

Figure 12: (a) isotropic (red) and VTI (green) reflectivity curves calculated with the lower layer filled with values found in the well, compatible with a water-saturated scenario. (b) Amplitudes picked in a shot gather near the well position for the same scenario. Amplitudes and reflection coefficients have coherent behavior and we see anomalous negative amplitudes at far offsets, just as the seismic, but intercept is positive and the AVO is a type II.

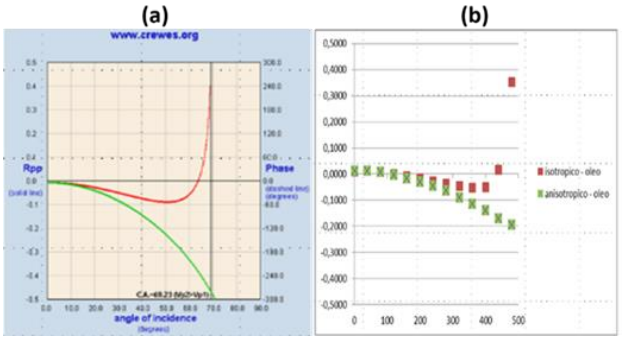

Figure 13: (a) isotropic (red) and VTI (green) reflectivity curves calculated with the lower layer filled with values obtained from a fluid substitution simulation, compatible with an oil-saturated scenario. (b) Amplitudes picked in a shot gather close to the well position for the same scenario. Amplitudes and reflection coefficient have similar behavior and the AVO anomaly is a type II / III.

Figures 12 and 13 are important to show that modeled amplitudes and expected reflection coefficients have a similar behavior. However, the oil-saturated scenario gives an AVO response closer to the real data than the real water-saturated scenario, which is confusing. A highly plausible explanation is that we inserted new properties only below the reservoir, and not above. In fact, the smooth model did not represent accurately the actual shale properties found in the well just above the reservoir. Therefore, we used the reflectivity calculator with more realistic properties values above the reservoir and found the curves shown in Figure 14 for the water and the oil-saturated scenarios. Since all previous simulations showed good correlation between modeled amplitudes and reflectivity curves, we have good reasons to believe that the curves shown in Figure 14 would be fairly reproduced if a full modelling were run again with updated models. The curves show that even the water-saturated scenario can generate an AVO type III response like the one seen in real data.

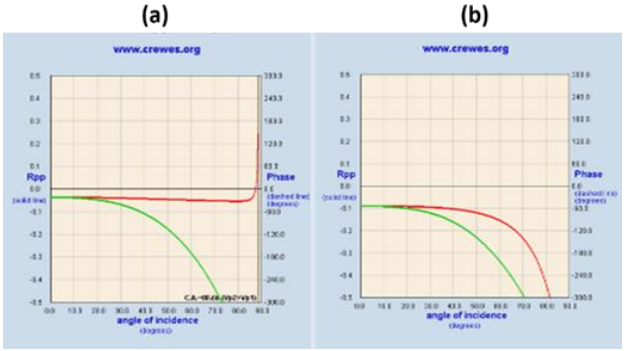

Figure 14: (a) isotropic (red) and VTI (green) reflectivity curves calculated with the upper layer filled with realistic values for the shale found in the well and the lower layer filled with water-saturated sandstone properties (also found in the well). (b) same curves generated with the

same values for the upper layer, but with oil-saturated properties in the lower layer. Both scenarios can generate AVO type III anomalies, as seen in real data.

We did not blame everything on anisotropy, though. In Figure 15, we present three intercept-gradient crossplots done with isotropic synthetics: (1) a water-saturated scenario with incidence angles from 0 to 40°, (2) an oil-saturated scenario with the same angle range, and (3) a water-saturated scenario with incidence angles from 0 to 65°. The dark blue, red and brown arrows indicate the top of reservoir for the three scenarios, respectively. The first scenario leads an AVO type IV response, just like Figure 2. When we replace water for oil, the AVO response is still a type IV, but more intense. However, if we allow higher incidence angles, the AVO response turns into a type III anomaly, even in a water-saturated scenario. This is an indication that the pitfall may be partially explained not only by anisotropy, but also by the presence of high incidence angles in the partial offset stacks.

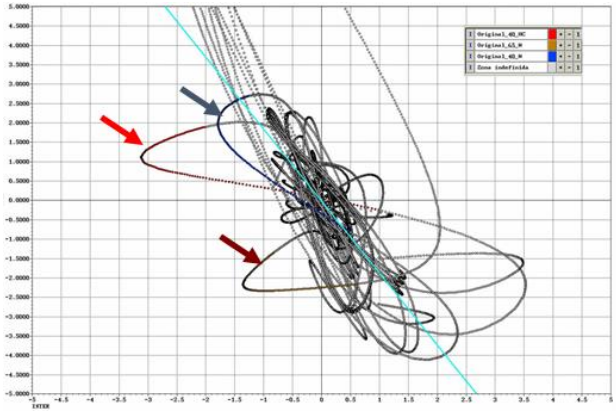

Figure 15: intercept-gradient crossplots for three scenarios, with arrows indicating the top of reservoir: water-saturated scenario with incidence angles from 0 to 40° (dark blue), oil-saturated scenario with the same angle range (red), and (3) a water-saturated scenario with incidence angles from 0 to 65° (brown). The presence of high incidence angles may help explain the AVO type III response seen in seismic data.

Conclusions

From Figure 10, we see that anisotropy can completely change the AVO response in this area and produce an amplitude behavior much closer to the real data. From Figures 11 to 13, we see that modelled amplitudes are coherent with reflectivity curves under different scenarios. From Figure 14a, we believe that the combination of an anisotropic shale just above a water-saturated isotropic sandstone can yield the AVO type III response seen in seismic data. From Figure 15, we believe that the potential presence of high incidence angles in the data may also help explain the pitfall.

Overall, anisotropy is definitely a major factor to consider during AVO analysis and its effect over the typical scenario of anisotropic shale over isotropic sandstone must not be despised: we believe this work is a good example.

Acknowledgments

Many people gave important contributions to this work. Fearing to forget someone, we thank Alcides Aggio, Andrea Damasceno, Celso Jardim, Cesar Calderon, Edimar Perico, Fabio Mendonça, Fernanda Darcle, Henrique Fraquelli, José Eduardo Lira, Julio Frigerio, Matheus Cafaro, Mauren Ruthner, Mario Sergio Costa, Paulo Carvalho, Roberto Dias, Victor Lebre and all others who helped. We also thank Petrobras and our managers for encouraging this work and authorizing the publication of this paper.

References

ALKHALIFFAH, T.; TSVANKIN, I. Velocity Analysis for Transversely Isotropic Media. Geophysics, V.60, No.5, p.1550-1566, 1995.

BACKUS, G. E. Long-wave elastic anisotropy produced by horizontal layering. J. Geophys. Res., 67, 4427-4440, 1962.

DALEY, P. F.; HRON, F. Reflection and transmission coefficients for transversely isotropic media. Bulletin of the Seismological Society of America, V. 67, No.3, pp 661-675, 1977.

IVANOV, Y.; STOVAS, A. Weak-anisotropy Approximation for P-wave Reflection Coefficient at the Boundary between Two TTI Media. 77th EAGE Conference & Exhibition, Madrid, 2015.

RUGER, A. P-wave reflection coefficients for transversely isotropic models with vertical and horizontal axis of symmetry: Geophysics, V.62, No.3, p.713-722, 1997.

SHUEY, R.T. A simplification of the Zoeppritz equations. Geophysics, Vol.50, No.4, p.609-614, 1985.

THOMSEN, L. Weak elastic anisotropy. Geophysics, V.51, No.10, p.1954-1966, 1986.

TSVANKIN, I. Seismic signatures and analysis of reflection data in anisotropic media. Elsevier, 2001.